ARTICLE OPEN

Check for updates

Adolescent mice exposed to TBI developed PD-like pathology in middle age

Rong Sha[1,2,3,7], Mingzhe Wu[2,4,7], Pengfei Wang[2,4,5,7], Ziyuan Chen[4], Wei Lei[1], Shimiao Wang[1], Shun Gong[1✉], Guobiao Liang[1,6✉], Rui Zhao[2,4,5✉] and Yingqun Tao[1,6✉]

Traumatic brain injury (TBI) is identified as a risk factor for Parkinson's disease (PD), which is a neurodegenerative disease characterized by the loss of dopaminergic neurons in the substantia nigra (SN). However, the precise mechanism by which chronic TBI initiates PD pathogenesis is not yet fully understood. In our present study, we assessed the chronic progression and pathogenesis of PD-like behavior at different intervals in TBI mice. More than half of the mice exhibited PD-like behavior at 6 months post injury. PD-like behavioral dysfunction and pathological changes were aggravated with the injured time extension in chronic phase of TBI. The loss of tyrosine hydroxylase positive (TH^+) neurons in the SN were partly associated with the accumulation of misfolded a-Synuclein and the cytoplasmic translocation of TDP-43 from nuclear. Moreover, the present of chronic inflammation was observed in SN of TBI mice, as evidenced by the enhancement of proinflammatory cytokines and reactive astrocytes and microgliosis post lesion. The enhanced phagocytosis of reactive microglia accounted for the reduction of dendrite spines. Our results revealed that chronic inflammation associated with the damage of TH^+ neurons and the development of progressive PD-like pathology after chronic TBI in mice. Our study shed new light on the TBI-triggered molecular events on PD-like pathology. Additional research is required to have a deeper understanding of the molecular factors underlying the impairment of dopaminergic neurons following TBI.

Translational Psychiatry (2025)15:27 ; https://doi.org/10.1038/s41398-025-03232-7

INTRODUCTION

Parkinson's disease (PD) is a prevalent neurodegenerative disorder that imposes a significant public health burden, impacting approximately 2–3% of those aged 65 years and older [1, 2]. Traumatic brain injury (TBI) is a prevalent form of mechanical injury, affecting an estimated 50 to 60 million people each year [3]. Notably, clinical evidences have shown that TBI is one of the risk factors in the development of PD [4–12]. These who encountered TBI during their early years are faced a heightened susceptibility to developing PD [9, 13].

The accumulation of α-Synuclein (α-Syn) in the substantia nigra (SN) has been identified as main contributor to PD-related pathology [14]. The degeneration of dopaminergic neurons reduces the function of the nigrostriatal pathway, leading to neurotransmission disorders and ultimately resulting in PD symptoms [15]. Previous studies report that mice performed poorly in open field test and present depression /anxiety-like behaviors at one month post-TBI, which is associated with the damage of dopaminergic neurons [16, 17]. The primary aim of the current study was to ascertain whether PD-like behavior is a late-onset symptom caused by TBI and its progression with the extended duration post TBI.

Inflammation occurs shortly after the initial TBI event (acute sequelae) and even persists for years in the affected areas [18]. Many studies document a significant loss of dopaminergic neurons following moderate TBI in rodents, which are accompanied by the enhancement of neuroinflammation [17, 19, 20]. The use of nonsteroidal anti-inflammatory drugs (NSAIDs) shows potential in mitigating the risk of PD and decelerating its progression, suggesting the potential involvement of neuroinflammation in the etiology of PD [21]. Microglia and astrocytes, which serve as the principal immune cells in the nervous system, have a significant impact on the regulation of neuroinflammation by releasing inflammatory cytokines and chemokines [22–24]. Nevertheless, the precise influence of reactive glial cells on neuronal functionality remains elusive in the SN post TBI.

The current work aims to explore the PD-like behavioral alterations and their probability of manifestation after TBI in mice. We undertook a thorough investigation on the onset of PD- like behavior and the loss of dopaminergic neurons in SN after TBI. Our study also specifically evaluates the effect of neuroinflammation of ipsilateral SN on behavior dysfunction in mice.

[1]Department of Neurosurgery, General Hospital of Northern Theater Command, Postgraduate Training Base of General Hospital of Northern Theater Command of Jinzhou Medical University, Shenyang, Liaoning, China. [2]Department of Forensic Pathology, China Medical University School of Forensic Medicine, Shenyang, Liaoning, China. [3]Department of Neurosurgery, The First Hospital of China Medical University, Shenyang, Liaoning, China. [4]Key Laboratory of Environmental Stress and Chronic Disease Control and Prevention, Ministry of Education, China Medical University, Shenyang, Liaoning, China. [5]Liaoning Province Key Laboratory of Forensic Bio-evidence Sciences, Shenyang, Liaoning, China. [6]China Medical University, Shenyang, Liaoning, China. [7]These authors contributed equally: Rong Sha, Mingzhe Wu, Pengfei Wang.
✉email: gongshunsmmu@foxmail.com; guobiaoliang@163.com; rzhao@cmu.edu.cn; yingquntao@163.com

Received: 28 February 2024 Revised: 8 December 2024 Accepted: 10 January 2025
Published online: 25 January 2025

MATERIALS AND METHODS

Animals

8–12-week-old male C57BL/6J mice ($n = 240$, weighing 18–25 g) were used in this study. Mice were housed under standard conditions (23 ± 1 °C, 12 h light–dark cycle and humidity is 60%). Mice were randomly allocated into TBI and age-match sham groups. Then mice were randomly sub-divided into eight experimental groups for four indicated time points (0, 1, 3 and 6 MPI), with thirty animals in each subgroup.

Controlled cortical impact (CCI) models

Briefly, an isoflurane anesthetized mouse was placed on a stereotaxic frame followed with surgical procedure. Briefly, a midline incision was made in the scalp to expose skull. A craniotomy with a diameter of 4 mm was conducted on the left cerebral hemisphere, which was precisely positioned 3 mm lateral to the midline and 3 mm posterior to bregma. A moderate TBI model was produced with craniocerebral strike apparatus (PinPoint PCI3000, Hatteras Instruments) using a 3 mm diameter impactor (velocity 1.5 m/s; duration 50 ms; depth 1 mm), as previously described [25]. After injury, the animals were placed in a 37 °C heated cage until recovery. Sham animals were subjected to surgery except for cortical impact.

Behavioral tests

Various behaviors are employed to identify PD-like behavior at indicated intervals post injury, including open field, tail suspension test, pole test, rotarod test, grip strength, and gait analysis.

Open field test (OFT). Mice were placed in a white acrylic box of 50 × 50 cm and allowed to freely explore for ten minutes. Their exploration trajectories were recorded using a camera. The box was wiped with 75% ethanol after each mouse trial to prevent the accumulation of olfactory cues. The open-field test was conducted by an examiner who was blinded to the treatment groups. The total distance of movement and the percent of time spend in the central area were calculated.

Rotarod. The rotarod test was generally practiced to investigate rodents' motor coordination and stability. Briefly, mice were forced to run at 10 rpm on a rotating rod to 40 rpm within 300 s. The latency to fall from the rotating rod is designated as the test's endpoint measure. Before the commencement of the study, animals were trained for the 5 consecutive days on the rotarod apparatus [26].

Pole test. The pole test apparatus consisted of a vertical pole with a diameter of 8 mm and a height of 50 cm, which placed in a cage with soft bedding. Mice were placed individually on top of the pole with their head oriented upward and allowed to descend to the floor [27]. Three pole descent trials were performed, and the mean time required for animals to descend to the base of the pole were used for analysis.

Grip strength. Mice were tested for strength using a grip dynamometer. The dynamometer is positioned horizontally, and the mice were supported by its tail and putted on the device. The measurement of peak grip force was conducted by instructing the mice to hold the metal grid and subsequently draw it back on a horizontal surface. The maximum grip force was documented until the mice experienced a loss of support. Each mouse was subjected to three trials of exhaustion, and the mean grip strength of the mice was calculated [27, 28].

Tail suspension test (TST). The TST test was performed as previously described to assess depressive-like behavior [29]. Mice were suspended by their tail (50 cm above the floor) using adhesive tape at 1 cm from the tip of the tail. The TST test was conducted and recorded for 6 min. TST data were recorded by the SMART™ tracking software program.

Gait analysis. Mice were subjected to gait assessment with the CatWalk XT automated gait analysis system (Noldus Information Technology, Wageningen, The Netherlands). A camera was used to record the footprints of mice in the glass walkway under a dark environment [30]. Only runs that were straight and uninterrupted were considered successful and were selected for further analysis. Any data failed to meet these criteria were excluded from the study.

Animal selection and sample collection

After conducting behavior test, we analyzed the behavioral parameters of age-matched sham mice and considered the 90% confidence interval as the baseline [31]. The motor abilities of TBI mice were assessed by comparing their performance to a baseline. All behavioral tests showed deviations from the baseline, indicating the presence of PD-like behaviors. In the TBI-6M group, mice displaying PD-like behavior were randomly selected for tissue analysis, while all 30 mice in the other groups were randomly chosen. The specific information about the mice was listed in Supplementary Table 3. Further experiments were conducted on the selected mice. The ipsilateral SN tissue was harvested and stored at −80 °C for protein and mRNA analysis after perfusing with cold phosphate-buffered saline. For immunostaining, mice were perfused with 4% paraformaldehyde. Parts of brain were embedded in paraffin and cut into 4 μm sections. Parts of brain were dehydrated in sucrose and cut into 50 μm sections.

Nissl staining

Briefly, the slides were dewaxed and stained within Nissl Staining Solution (Beyotime Biotechnology, Shanghai, China) for 20 min. After, rinsing with ddH_2O, the sections were decolorized in 75% ethanol, cleared in xylene, and sealed with neutral resin. Finally, the sections were observed using light microscope (Olympus DP74, Tokyo, Japan).

Western blotting

The ipsilateral SN tissues were rinsed with cold PBS followed by homogenized in the RIPA lysis buffer containing phenylmethanesulfonyl fluoride (PMSF) (Beyotime, Shanghai, China). The lysates were centrifuged and total protein concentration was evaluated with Enhanced BCA Protein Assay Kit (Beyotime, Shanghai, China). Samples were separated by using a Bis-Tris gel and then transferred onto polyethylene difluoride (PVDF) membranes blocked with milk for 2 h at room temperature (RT). The membranes then incubated with antibodies subsequently at RT and were imaged with the ECL (Tanon 5500, Shanghai, China). The antibodies used in this study were listed in Supplementary Table 1.

Immunofluorescence

Coronal brain sections were dewaxed and incubated in blocking solution containing 5% donkey serum and 0.5% Triton X-100 in PBS at RT, then incubated with primary antibodies at 4 °C overnight. Slice were rinsed in PBS followed by incubation with Alexa-Fluor-conjugated secondary antibodies at RT. Slices were then washed and mounted with Fluor-mount contained nuclear marker DAPI. Images were acquired with 1 μm step size at ×200 magnification using a Zeiss Axio Scan Z1 confocal microscope system (Zeiss, Jena, Germany). Each area was randomly selected and the cells were manually counted by two blinded investigators. Percentage of positive area and area of cell soma were quantified by Image J software. The antibodies we used for immuno-staining were listed in Supplementary Table 1.

qReal-time PCR

Total RNA samples were extracted from SN tissue using TRIzol regent (279510, Thermo Fisher Scientific, USA), and first-stand cDNA was generated using the PrimeScript™ RT reagent kit (TRR047A, Takara Biotechnology, Japan). qReal-time PCR (qPCR) was performed using SYBR® Premix Ex Taq™ II RT-PCR kit (RR820A, Takara Biotechnology, Japan) for quantity analysis of the mRNA. All reactions were performed in triplicates and the mRNA levels were normalized to *Gapdh*. The primer sequences which we used are listed in Supplementary Table 2.

Quantification of cytokine levels

Enzyme-linked immunoassay kits (Mlbio, China) were used to measure the levels of IL-1β, IL-6 and TNF-α in SN tissues according to the technical instructions supplied by the ELISA kits [32].

TUNEL assay

Apoptotic nuclei were detected in SN region using an TUNEL Bright Green Apoptosis Detection Kit (Vazyme, China) according to manufacturer's instructions. The number of apoptotic cells in the SN were counted by Image-J software (version 2.0; National Institutes of Health, Bethesda, MD, USA).

Sholl analysis of the morphology of astrocyte

Sholl analysis was conducted to investigate the astrocytic and microglial morphology in the frozen section of SN as previously described [33]. Briefly, Z-stack images were collected with a 60 × oil immersion lens with 2.5 µm step size, and only cell that exhibited a distinct cell body and processes that did not extended beyond the field of view were chosen for analysis. For each animal, more than 4 astrocyte and microglia were selected from the ipsilateral SN area. Each image was analyzed with a Sholl analysis plugin in Fiji. We used the line segment tool to draw a line from the center of each soma to their longest process. We set every shell in 3 µm (for astrocyte) or 2.5 µm (for microcyte) steps to determine the number of intersections at each Sholl radius [33].

Golgi staining and analysis

Neuron staining was performed using the FD Rapid Golgi-Stain Kit (FD Neuro Technologies) as per the manufacturer's instructions to histologically investigate dendritic spines under light microscopy (Olympus DP74, Tokyo, Japan). In short, mice brains were removed, and processed for Golgi staining following the manufacturer's manual. The brains were later sectioned into 100 µm slices using a freezing microtome (POLAR-D-JC, Tissue-Tek). The sections were then mounted on gelatin-coated slides (FD Neuro Technologies) with solution C and stained. Combination of images of the spines were created by combination of multiple microscopic photographs taken with a 64 × oil immersion lens. The spines were manually counted in ImageJ and the number of spines per 10 mm length was calculate. The various spine shapes were counted in the same dendritic segments and classified based on the morphology of their head and neck into four categories: thin, stubby, mushroom and filopodial-like.

Statistical analysis

The data was expressed as mean ± standard deviation (SD). The positive cells in SN were counted and analyzed by researchers who were not directly involved in the experiment. The quantification of positive cells was counted using ImageJ software. Student's *t* test was used to compare data between sham and TBI groups. Mann-Whitney U test was used to compare data between two groups with non-normal distributed data. Two-way analysis of variance (ANOVA) was used to compare the difference between sham and TBI groups of different time point, followed by Tukey's post hoc tests for multi-group comparisons. Correlation analyses were conducted using Pearson tests following the assessment of the Gaussian distribution of values. GraphPad Prism 8.0 (GraphPad Software Inc, CA, USA) was used to perform the statistical analyses. A $p < 0.05$ was considered statistically significant.

RESULT

TBI led to defects in motor function and anxiety/depression-like behavior

We established a model in adolescent (8–12 weeks old) mouse and investigated the PD-like behavior alterations during the chronic phase of TBI. The mice were subjected to a range of behavioral tests and there was no significant alternation in motor function among Sham mice at all indicated time points. Meanwhile, a significant decrease in both the total distance of voluntary movement and the proportion of time spent in the center area during the Open Field Test were found at 3 and 6 months' post-injury (MPI), as shown in Fig. 1B–D. The duration of rest in TST exhibited a notable increase at 3 and 6 MPI (Fig. 1E), indicating that mice developed depressive-like behavior. In rotarod test, the initial latency to fall decreased at each timepoint after TBI. Moreover, the time spent on the rotarod in 6 MPI group was considerably lower compared with that in 3 MPI (Fig. 1F). Additionally, compared with the age-matched Sham mice, the grip strength was significantly reduced at 3 MPI and 6 MPI (Fig. 1G). Results from gait analysis system showed significant and continuous alteration in four limbs for mice following injury and the defect of right-side limbs were more severe than that of left-side limbs (Fig. 1I, J, Supplementary Fig. 1A–C). Mice in 6 MPI exhibited bigger reduction in stride length paw swing time of limbs, the maximum contact area of mice accompanied with an extended duration of stand time (Fig. 1H–J; Supplementary Fig. 1A, B). At 6 MPI, the base of support (BOS) of forelimbs significant reduced, while the distance between the two hind limbs was greater (Supplementary Fig. 1C). We also calculated the ratio of abnormal behaviors, 53.3% of the TBI mice exhibited poor performance in all the conducted tests, indicating significant PD-like behaviors at 6 MPI (Supplementary Fig. 1D). Our behavior data indicates the progressive behavioral deficits after injury and more than half of the TBI mice present the PD-like behaviors in mice 6 months after TBI.

Apoptosis is related to dopaminergic neurons loss after chronic TBI

Given that dopaminergic neuron exhibits regulatory effects on locomotion, the effects of dopaminergic neurons loss in the substantia nigra pars compacta (SNc) by TBI was assessed. Results from Nissl staining showed that the number of Nissl bodies in the SNc of mice was significantly reduced after TBI, accompanied by the occurrence of neuronal pyknosis in the SNc (Fig. 2B). Western blotting showed that the protein level of TH was significantly decreased in TBI group compared with the age-match group at 6 MPI, while no significant alternation at 1 and 3 MPI (Fig. 2C, D). In line with this, there was a significant reduction in the number of TH-positive neurons (Fig. 2E, F). To explore whether apoptosis would explain the decrease of dopaminergic neurons in TBI mice, we performed double staining of TH and TUNEL. As shown in Fig. 2E, G, there was persistent TUNEL staining colocalized with TH at the indicated timepoints in the TBI mice. Our data suggests apoptosis would be partly accounted for the loss of dopaminergic neurons caused by chronic TBI.

TBI induced the aggregation of protein in SN following TBI

Previous studies have shown that abnormal accumulation of α-Synuclein in dopaminergic neurons is one of the key pathological changes in PD [34, 35]. We then explored the expression level of α-Synuclein by immunofluorescence staining and western blotting in ipsilateral SN post injury. As shown in Fig. 3A, B, protein level of α-Synuclein was enhanced in the SN of chronic TBI at 1, 3, 6 MPI compared with age-matched Sham mice. In line with the data of western blotting, the number of α-Synuclein (+) dopaminergic neurons in chronic TBI mice at 1, 3, 6 MPI was higher than that of the age-matched control group (Fig. 3C–E). Positive α-Synuclein signals were found to be adjacent to the nucleus in the cytoplasm and along neurites of dopaminergic neurons in the SNc (Fig. 3C). Furthermore, the number of α-Synuclein (+) and TH (+) neurons was counted and plotted separately to explore the correlation between dopaminergic neuronal loss and the accumulation of α-Synuclein in the chronic TBI model. A positive correlation between time and the ratio of TH + α-Syn double positive neurons/TH (+) neurons by Pearson's correlation analysis, with a R^2 value of 0.9088 (Fig. 3F). In addition, it has been proved that TDP-43 undergoes nuclear translocation and facilitates neuronal damage in several neurodegenerative diseases [36, 37]. Our present study indicated that TDP43 exhibited mislocalization in the cytoplasm at 1 MPI by double immunofluorescence and demonstrated strongly cytoplasm translocation and nuclear clearing in TH (+) neurons of SNc at 6 MPI. (Fig. 3G; Supplementary Fig. 2A, B). Our results demonstrate the abnormal accumulation of α-Synuclein and cytoplasm translocation of TDP-43 in dopaminergic neurons may partly be related to the PD-like behavior in chronic TBI mice.

TBI induced long-lasting neuroinflammation in ipsilateral SN

Subsequently, we conducted an evaluation of the neuroinflammatory response in the ipsilateral SN following injury through the measurement of protein and mRNA of pro-inflammatory cytokines, including interleukin (IL)-1β, IL-6, and tumor necrosis factor-alpha (TNF-α). The data demonstrated a significant increase in the protein and mRNA concentrations of IL-1β, IL-6, and TNF-α in chronic TBI mice as compared to age-matched sham mice at each indicated timepoints (Fig. 4A–F). Our study

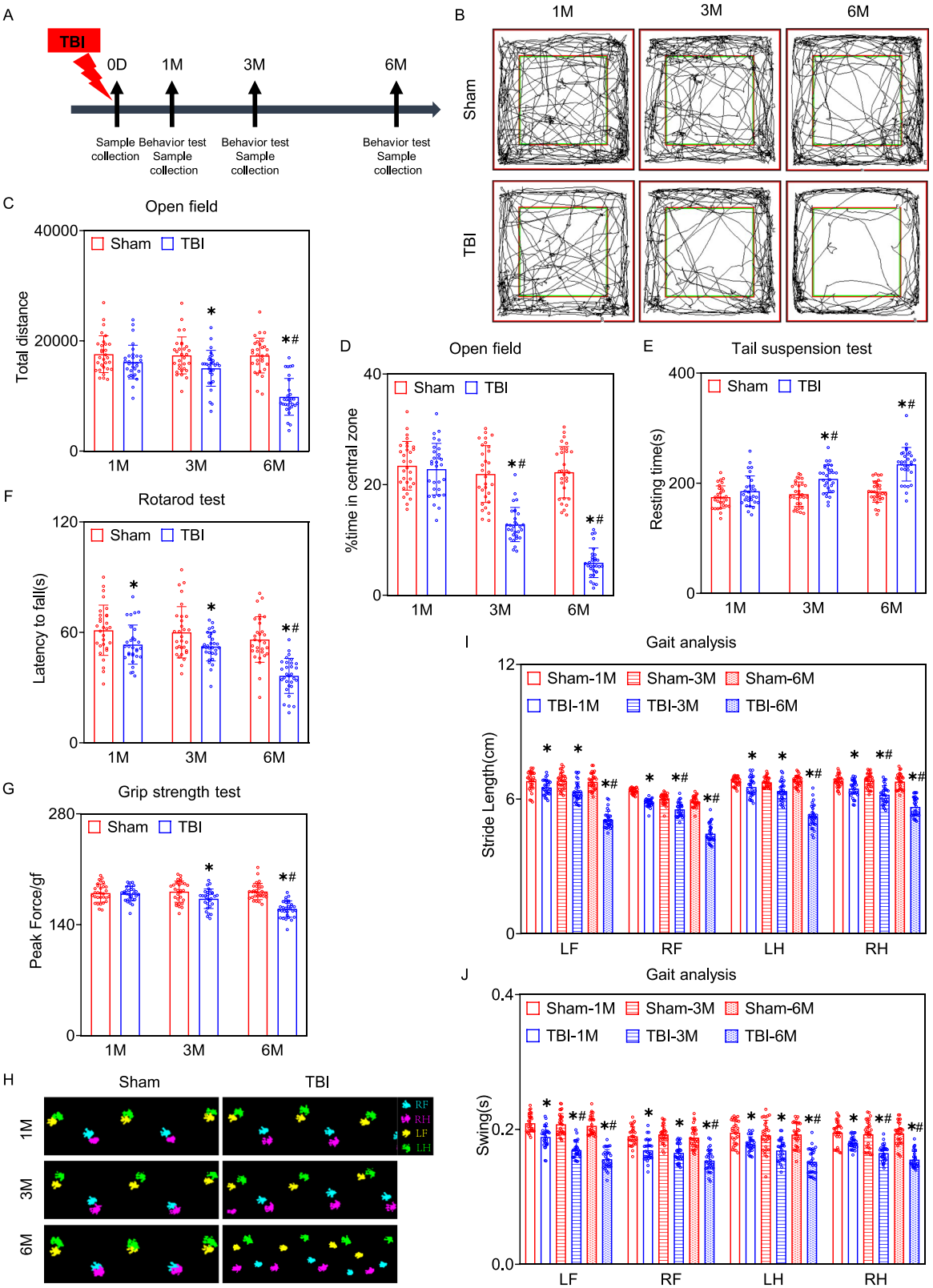

Fig. 1 The alteration of motor function and anxiety/depression-like behavior in mice in chronic TBI mice. A Time course schema for behavioral test and sample collection. **B** The representative motion trajectory diagram of OFT at 1, 3 and 6 MPI. **C** Statistical analysis of total distance of voluntary movement. **D** Statistical bar of percentage of time in central zone. **E** The resting time in TST at 1, 3 and 6 MPI. **F** First latency to fall in rotarod test. **G** The peak force at 1, 3, 6 MPI. **H** The representative paw prints in gait analysis. **I** Statistical analysis of stride length in gait analysis at 1, 3 and 6 MPI. **J** Statistical analysis of swing in gait analysis at 1, 3 and 6 MPI. The data was represented as means ± SD; $n = 30$. *$p < 0.05$ vs. age-match sham group (Mann-Whitney U Test); $^{\#}p < 0.05$ vs. preceding adjacent TBI group (two-way ANOVA followed by Tukey's *post hoc* test).

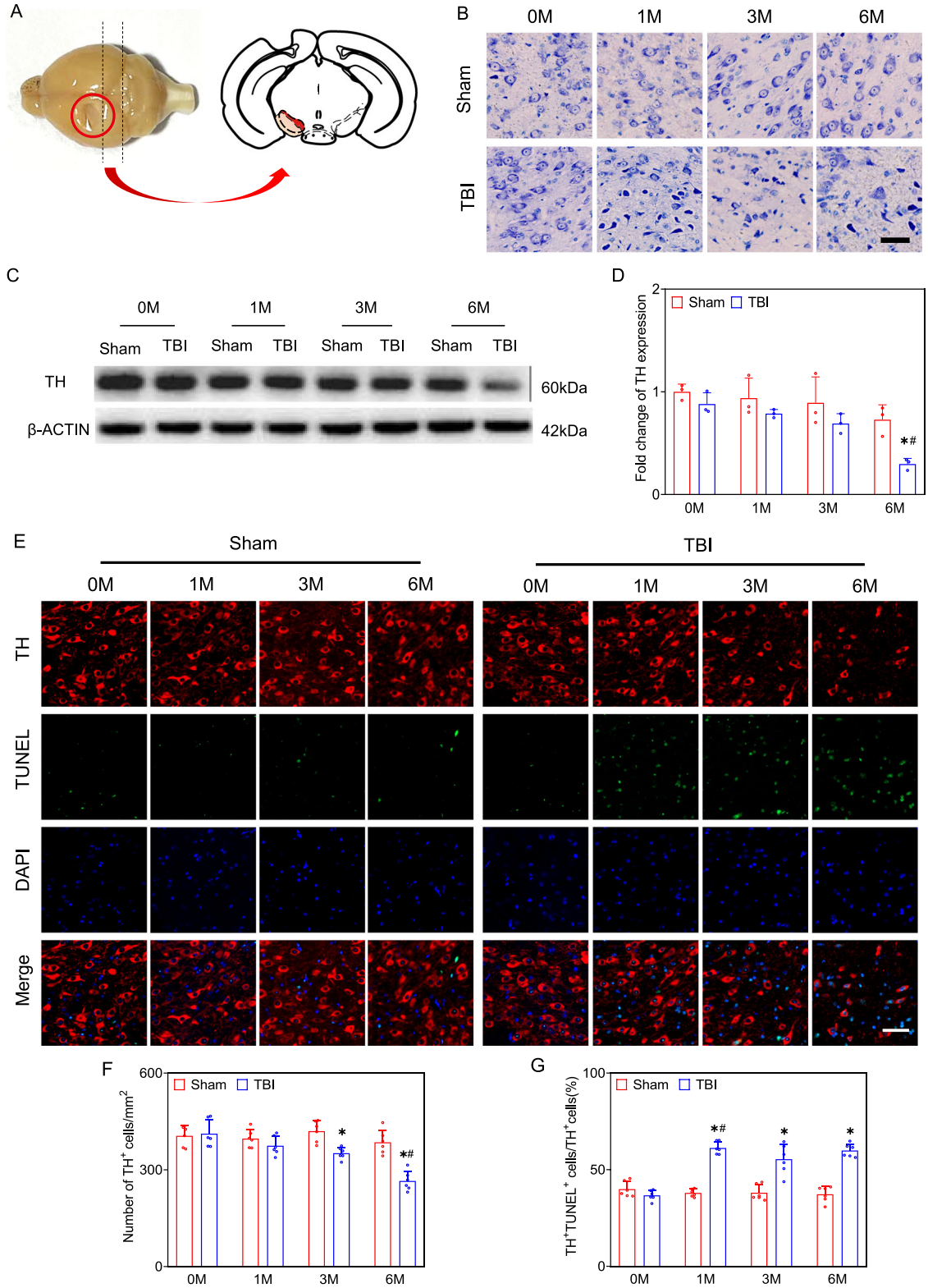

Fig. 2 Apoptosis is related to the dopaminergic neurons' loss in the SNc following TBI. A The region of TBI and a transverse section of SNc. **B** Represent images of Nissl-staining in SN, $n = 6$, scale bar = 50 μm. **C**, **D** Representative Western blotting of TH in the SN, $n = 3$. **E**–**G** Representative immunofluorescent images of TH (red) and TUNEL (green) in SNc, and statistical analysis of number of TH and TUNEL double positive cells, $n = 6$, scale bar = 50 μm. *$p < 0.05$ vs. age-match sham group (Student's t test); #$p < 0.05$ vs. preceding adjacent TBI group (Two-way ANOVA followed by Tukey's *post hoc* test). The values were represented as means ± SD.

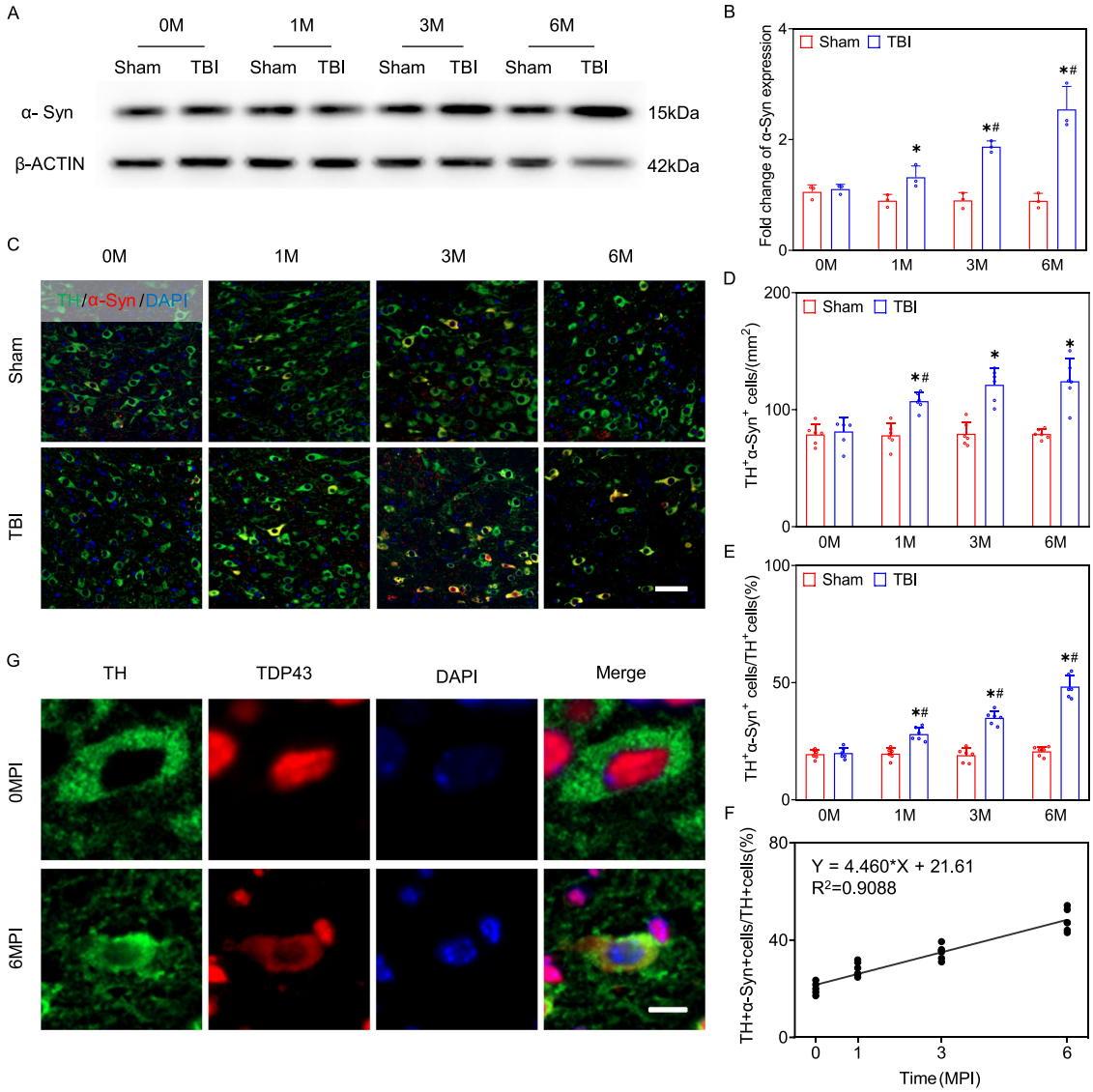

Fig. 3 The aggregated α-Syn and nuclear clearing of TDP-43 in dopaminergic neurons during the chronic phase of TBI. **A**, **B** Representative Western blotting and the relative intensity of α-Syn, $n = 3$. **C** Representative images immunofluorescence double staining of TH (green) and α-Syn (red) in the SNc of Sham and TBI mice at different timepoints post injury, $n = 6$, scale bar = 50 μm. **D** Quantification of TH and α-Syn double positive neurons in the SNc in chronic TBI. **E** Quantification of the proportion of TH + α-Syn double positive cells in total TH (+) cells in the SNc. **F** Correlation analysis between the ratio of TH + α-Syn double positive neurons to TH (+) neurons and post injured intervals, $n = 6$. **G** Representative co-localization images of TH (green) and TDP-43(red) in the SNc region of the mice at 6MPI, $n = 6$, scale bar = 10 μm. *$p < 0.05$ vs. age-match sham group (Student's t test); # $p < 0.05$ vs. preceding adjacent group (Two-way ANOVA followed by Tukey's *post hoc* test). The values represent the means ± SD.

indicates the persistent enhanced inflammation in the ipsilateral SN during chronic TBI.

Persistent reactive astrocytes in SN region of chronic TBI mice

To assess the reactive astrocyte, we detected the expression of glial fibrillary acidic protein (GFAP) in the SN. Our findings indicated a significant increase of GFAP protein level in the ipsilateral SN at all indicated timepoints post TBI compared with the age-matched sham mice (Fig. 5A, B). Furthermore, the number of astrocytes and positive area of GFAP immunostaining were increased after TBI and reached their peak levels at 3 MPI in chronic TBI mice (Fig. 5C, E, F). In addition, we employed another astrocytic marker S100β to evaluate the reactive astrocytes in chronic TBI. The number of S100β + GFAP double positive cells was also increased in the SN at 1, 3, 6 MPI compared with the age-matched sham mice (Supplementary Fig. 3A, B). Then, in order to evaluate the development of neurotoxic A1 reactive astrocytes in the chronic TBI mice model, C3d was co-stained with GFAP. As shown in Fig. 5D, G, the ratio of C3d (+) astrocytes was increased in TBI mice at all indicated timepoints. The morphological changes of the reactive astrocytes in the SN were further evaluated by Sholl analysis, a common technique to measure the arborization of cells by measuring the total numbers of intersections and the maximum process extension length [33]. In TBI mice, a more intricate branching pattern of astrocyte was observed in TBI mice than those in age-matched sham mice. Reactive astrocytes in ipsilateral SN of TBI mice exhibited a higher quantity of intersections, greater arborization, longer reaching extension, which reached their maximum of complexity at 3 MPI in TBI mice (Fig. 5H–K). These findings suggest that reactive astrogliosis damages neurons by setting up a toxic environment and losing support.

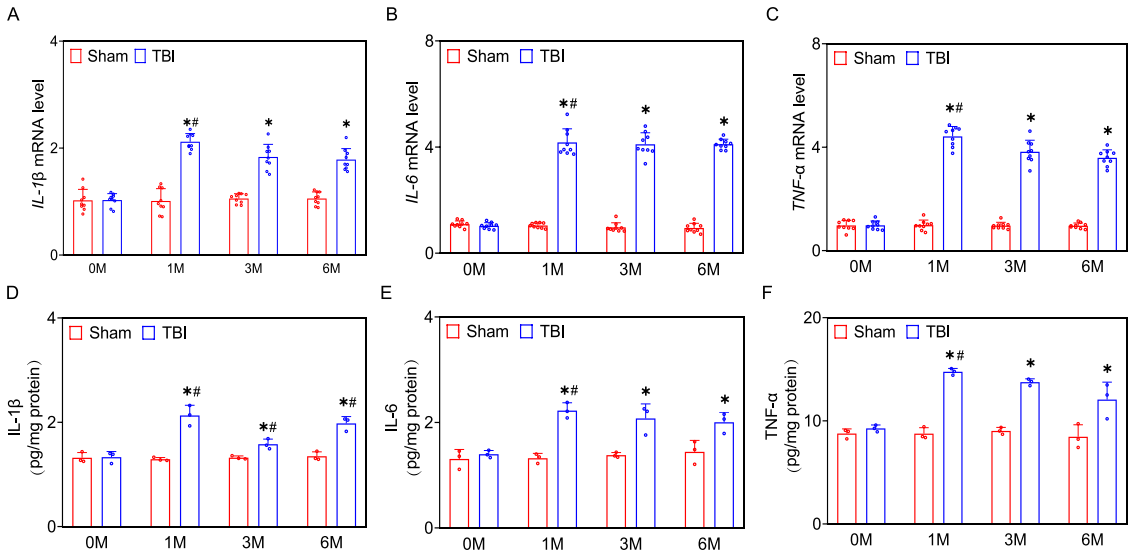

Fig. 4 Persistent enhancement of pro-inflammatory cytokines in the SN during chronic TBI. A–C qRT-PCR of mRNA expression of *IL-1β*A, *IL-6*B, *TNF-α*C in the SN post injury, $n = 9$. **D–F** The protein levels of IL-1βD, IL-6E, TNF-αF in the SN during chronic TBI, $n = 3$. $^{*}p < 0.05$ vs. age-match sham group (Student's *t* test); $^{\#}p < 0.05$ vs. the preceding adjacent group (Two-way ANOVA followed by Tukey's *post hoc* test). The values represent the means ± SD.

Reactive resident microglia in response to chronic TBI in the SNc

In addition, we evaluated the reactive microglia and the phagocytic function in the SNc by immunostaining. In Sham group, IBA1 (+) cells were dominated by a branching phenotype with a few hypertrophic and bushy cells, while the IBA1 (+) cells closed to damaged neurons exhibited significant increase in the cell density and enlarged cell soma (Fig. 6A–C). TMEM119 is a type I transmembrane protein specifically expressed by resident microglia in the healthy brain [38]. Double immunostaining of IBA1 with TMEM119 revealed that all the IBA1 (+) cells were labeled with TMEM119, indicating that resident microglia, rather than peripheral macrophages, contributed to the inflammatory response in the SNc of chronic TBI (Supplementary Fig. 3B, D). We then evaluate the polarization of microglia using double immunostaining of CD16/32 + IBA1 and ARG-1 + IBA1. As shown in Fig. 6D, E, both M1 and M2 subtypes of microglia were increased after chronic TBI. A greater proportion of reactive microglia tended to the transformation into the M1 subtype, as shown in Fig. 6H. The protein levels of IBA1, CD16/32 and ARG-1 showed the comparable results (Fig. 6F, Supplementary Fig. 4C). Additionally, we conducted a separate, in-depth analysis of the IBA1 immunopositive microglia to investigate the microglial changes associated with elevated inflammation levels in the SNc of TBI mice. Subsequent Sholl analysis revealed significant differences in the branching patterns of microglia between TBI and age-matched sham mice, with TBI mice having significantly fewer branch intersections at distances of 5–40 μm from the cell soma. Furthermore, the total length of microglia processes was shorter and the sum of intersections was reduced in the TBI mice, indicating substantial process retraction. Our data demonstrated that the reactive resident microglia might contribute to the dopaminergic neuronal damage in chronic TBI mice.

Enhanced phagocytosis of reactive microglia after TBI

To substantiate the hypothesis that reactive microglia in the PD-like behavior triggered by chronic TBI is linked to compromised synaptic dysfunction in TBI mice, we conducted the following experiments. Firstly, double immunostaining of IBA1 with CD68 was employed to assess the phagocytic function of the reactive microglia. As shown in Fig. 7A, CD68 was undetectable in mice of 0 and 1MPI. In contrast, the expression of CD68 was upregulated in IBA1^{+} cells and presented a significant increase at 6 MPI (Fig. 6A, B, Supplementary Fig. 4D). Next, we detected the colocalization of postsynaptic marker PSD95 with IBA1 in the SNc of chronic TBI mice. The enhanced overlaid signal in Fig. 7C demonstrated that reactive microglia engaged in the phagocytosis of synapses in the 3 and 6 MPI mice (Fig. 7C–E, Supplementary Fig. 4E). The protein levels of PSD95 showed the comparable results (Fig. 7F, G). Further study revealed the dendritic spine density exhibited a notable drop over the chronic duration of TBI when compared with age-matched sham mice (Fig. 5H, I). Analysis of the density of the different structures, including thin, stubby, mushroom or filopodial-like spines, revealed a notable decrease in stable mushroom and stubby spines among neurons in the SNc with TBI (Fig. 5J). Our study indicates that the enhanced engulfment of synapse by reactive microglia related to motor defects and TH+ neuronal loss during the chronic TBI.

DISCUSSION

TBI is one of the environmental factors for the development of PD and related disorders due to the critical changes impacting brain cognition and motor function that occur over an extended time period after TBI [12]. This current study demonstrated that adolescent TBI led to progressive motor function dysfunction in mice and more than half of the mice displayed behavior features similar to PD in middle-age. Additionally, accumulation of misfolded α-Syn and the removal of TDP-43 from nuclear contributed to the apoptosis of dopaminergic neurons in mice with motor dysfunction. Furthermore, we observed persistent production of pro-inflammatory cytokines, reactive astrocytes and microgliosis in the ipsilateral SN. It is worth mentioning the phagocytosis of microgliosis participated in the elimination of dendrite spines. In summary, this study provided evidence and potential mechanism that moderate TBI had the potential to initiate a gradual development of PD-like pathology, as illustrated in Fig. 8.

Extensive research in the field of TBI focus on neurocognitive and neuropathological changes post TBI and the risk of developing neurodegenerative diseases [39]. PD is characterized by severe motor dysfunction including muscular rigidity, resting

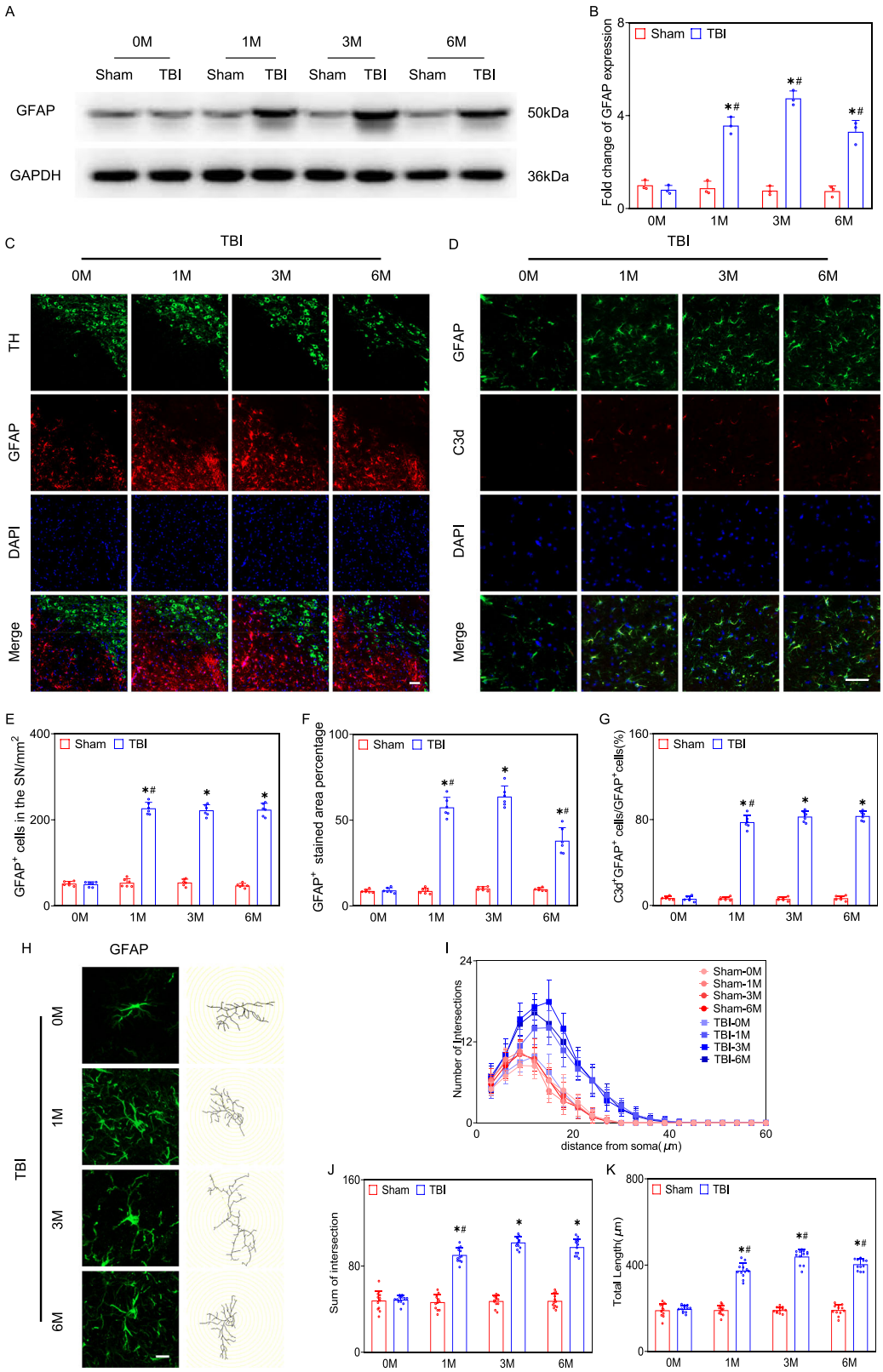

tremor and bradykinesia [6, 40]. We found that adolescent TBI led to bradykinesia and anxiety/depression-like behavior which aligned with previous studies [17, 41]. Depressive and anxiety are commonly coexisting and common in people with PD. Besides, TBI mice showed progressive balance impairment, decreased muscle strength and abnormal gait. Inline with the observations in experimental TBI mice, the intensity and contact area of the paws are also reduced in animal models of PD [30]. At the same time, an increase in swing duration and a decrease in swing speed of the hindlimbs has been reported in PD animals [30]. PD patients adapt

Fig. 5 Reactive astrocytes during the chronic phase of TBI. A Representative Western blotting image of GFAP in SN of TBI mice and their age match sham mice, $n = 3$. **B** The relative density of GFAP protein in SN. **C** Representative double immunostaining of GFAP (green) and TH (red) in the SN of TBI mice at different timepoints post injury, scale bar = 50 μm, $n = 6$. **D** Representative immunofluorescence staining of GFAP (green) and C3d (red) in the SN, scale bar = 50 μm, $n = 6$. **E** Quantification of GFAP positive cells in the ipsilateral SN of chronic TBI mice. **F** GFAP positive area in the SN. **G** The ratio of GFAP and C3d double positive cells to GFAP (+) cells in the SN. **H** Representative 3D morphological reconstruction of astrocyte in mice, scale bar = 10 μm, $n = 12$. **I–K** Sholl analysis of morphological complexity of astrocytes in the SN at different time. The change of number of intersectionsI, total lengthJ, and sum of intersectionK had the time sequence regularity. $^{*}p < 0.05$ vs. age-match sham group (Student's *t* test); $^{\#}p < 0.05$ vs. preceding adjacent group (Two-way ANOVA followed by Tukey's *post hoc* test). The values represent the means ± SD.

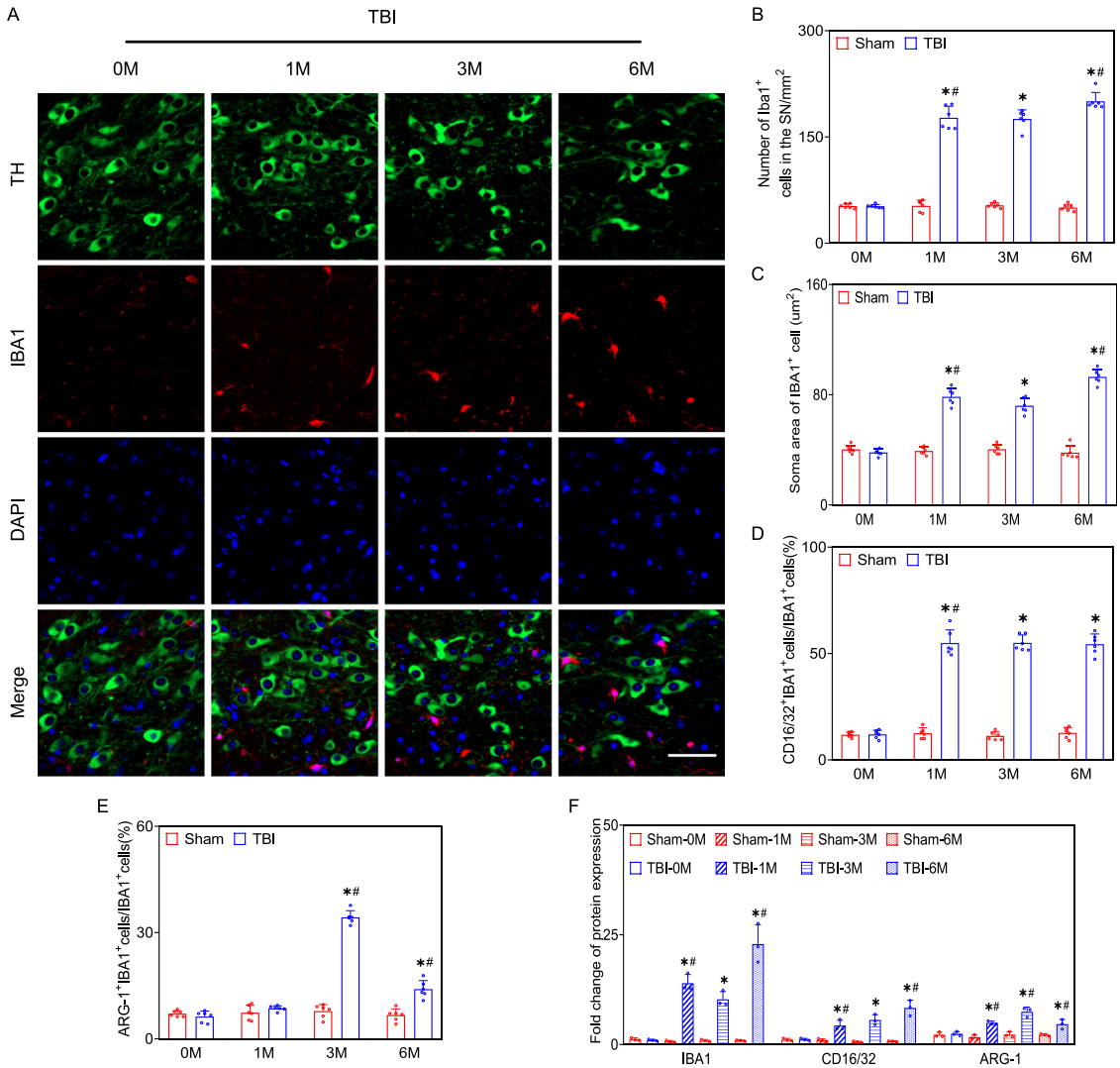

Fig. 6 Resident microglia were reactive in the SNc of chronic TBI mice. A Representative images immunofluorescence double staining of IBA1 (red) and TH (green) in the SNc of TBI mice at different time point post injury, scale bar = 50 μm, $n = 6$. **B** Quantification of IBA1 positive cells in the SNc. **C** Soma area of IBA1 (+) cells in the SNc, $n = 6$. **D, E** TBI altered the polarization of microglia M1/M2 during the chronic phase of TBI, $n = 6$. **F** Analyzes of Western blotting of IBA1, CD16/32, ARG-1 in the SNc, $n = 3$. $^{*}p < 0.05$ vs. age-match sham group (Student's *t* test); $^{\#}p < 0.05$ vs. preceding adjacent group (Two-way ANOVA followed by Tukey's *post hoc* test). The values represent the means ± SD.

their coordination patterns by adjusting walking speed, but this adaptation is limited due to rigidity and bradykinesia, which are associated with degeneration of the dopaminergic system [42]. In an attempt to better understand the relationship between TBI and PD, we hypothesized that any alteration in the post-injury dopaminergic system could have significant effects on long-term PD-like features. The degeneration of dopaminergic terminals and axons were occurred before the demise of dopaminergic neurons in the SN, which finally led to the clinical symptoms of PD [43–45]. Previous studies demonstrated a reduction of TH-positive neurons in the ipsilateral SNc after TBI [17, 19, 46]. Nevertheless, there exists a scarcity of data pertaining to the specific pattern of cell death in the ipsilateral SN during the chronic phase of TBI. Our study revealed that apoptosis was accounted for responsible for the long-lasting dopaminergic neurons loss in the ipsilateral SN post TBI. Furthermore, secondary apoptotic damages appeared to be more severe than primary damage neurons and affected sites distant from the impact. In future studies, it would be valuable to explore whether neurons in the SN undergo other forms of cell death, such as pyroptosis and necrotic apoptosis during the

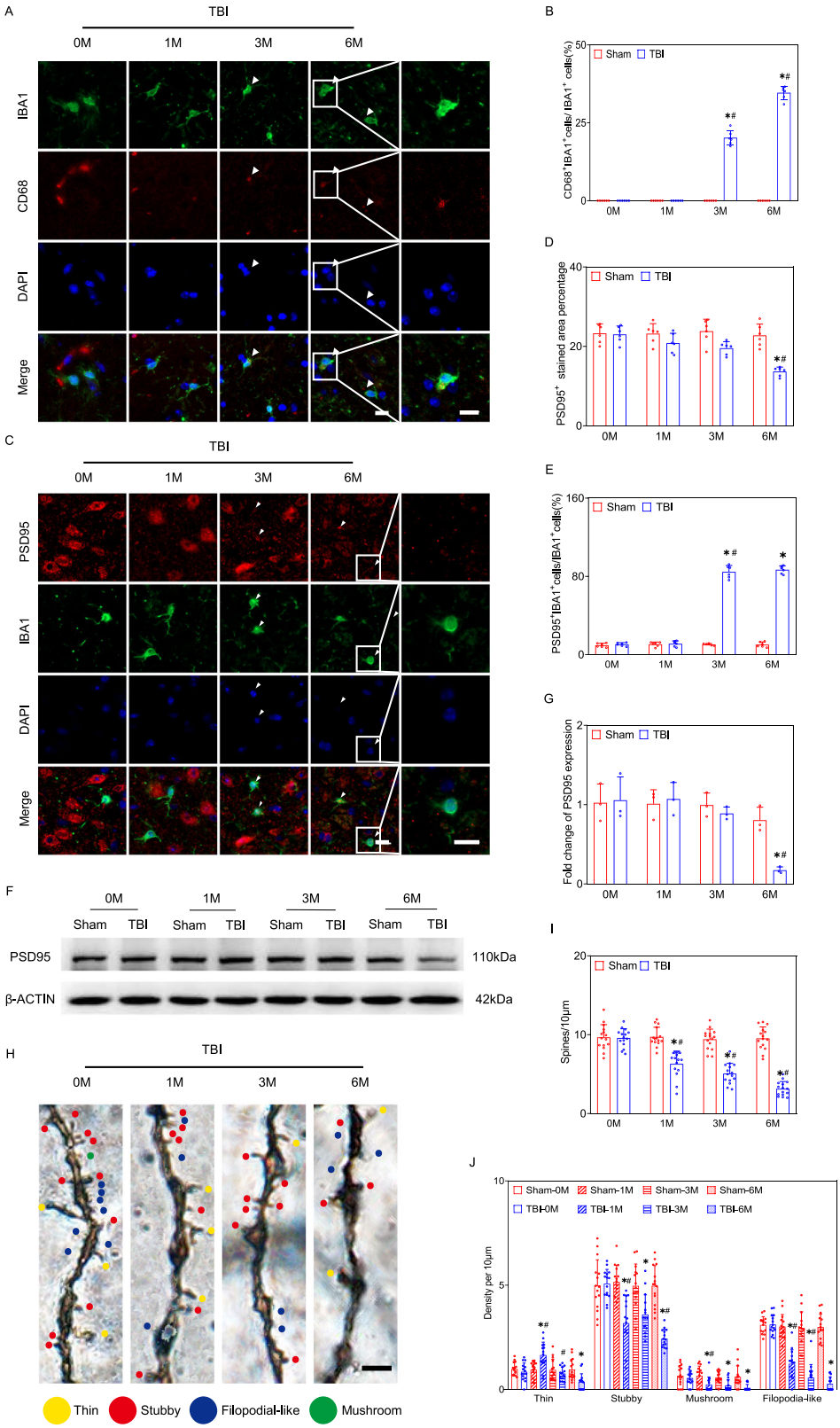

chronic phase of TBI, which would contribute to a better understanding of the pathogenesis of PD.

TBI leads to complex chronic pathology, including neuronal degeneration, persistent inflammation, and misfolding of proteins such as α-Syn, amyloid precursor protein (APP), Tau, and TDP-43 [4, 46, 47]. Accumulation of misfolded α-Syn is thought to play a crucial role in the pathophysiology of PD [48]. Sandra A. Acosta conducts a seminal study that establishes the role of α-Syn as the pathological link between TBI and PD [46]. Our results demonstrated progressive accumulation of α-Syn within TH-positive

Fig. 7 Reactive Microglia engulfed synapses in the chronic phase of TBI. A Representative images immunofluorescence double staining of CD68 (red) and IBA1 (green) in the SN of TBI mice at different time point post injury, scale bar = 10 μm, $n = 6$. **B** The ratio of IBA1 + CD68 double positive cells to IBA1 (+) cells in the SNc. **C–E** Representative images of immunofluorescence double staining of PSD95 (red) and IBA1(green) in the SNc of TBI mice at different time point post injury, scale bar = 10 μm, $n = 6$. **F** Representative Western blotting image of PSD95 in the SN of TBI mice and their age match sham mice, $n = 3$. **G** The relative density of PSD95 protein in the SN. **H** Representative images of Golgi-Cox staining in the SNc at different timepoints post injury. Yellow dots for counting thin dendritic spines, red dots for counting stubby dendritic spines, blue dots for counting filopodial-like dendritic spines, green dots for counting mushroom dendritic spines, scale bar = 2 μm, $n = 15$. **I** The number of spines per 10 μm dendritic length was quantified at different time point post injury. **J** The number of thin, stubby, mushroom or filopodia shaped spines were quantified per 10 μm dendritic length. $^{*}p < 0.05$ vs. age-match sham group (Student's *t* test); $^{\#}p < 0.05$ vs. preceding adjacent group (Two-way ANOVA followed by Tukey's *post hoc* test). The values represent the means ± SD.

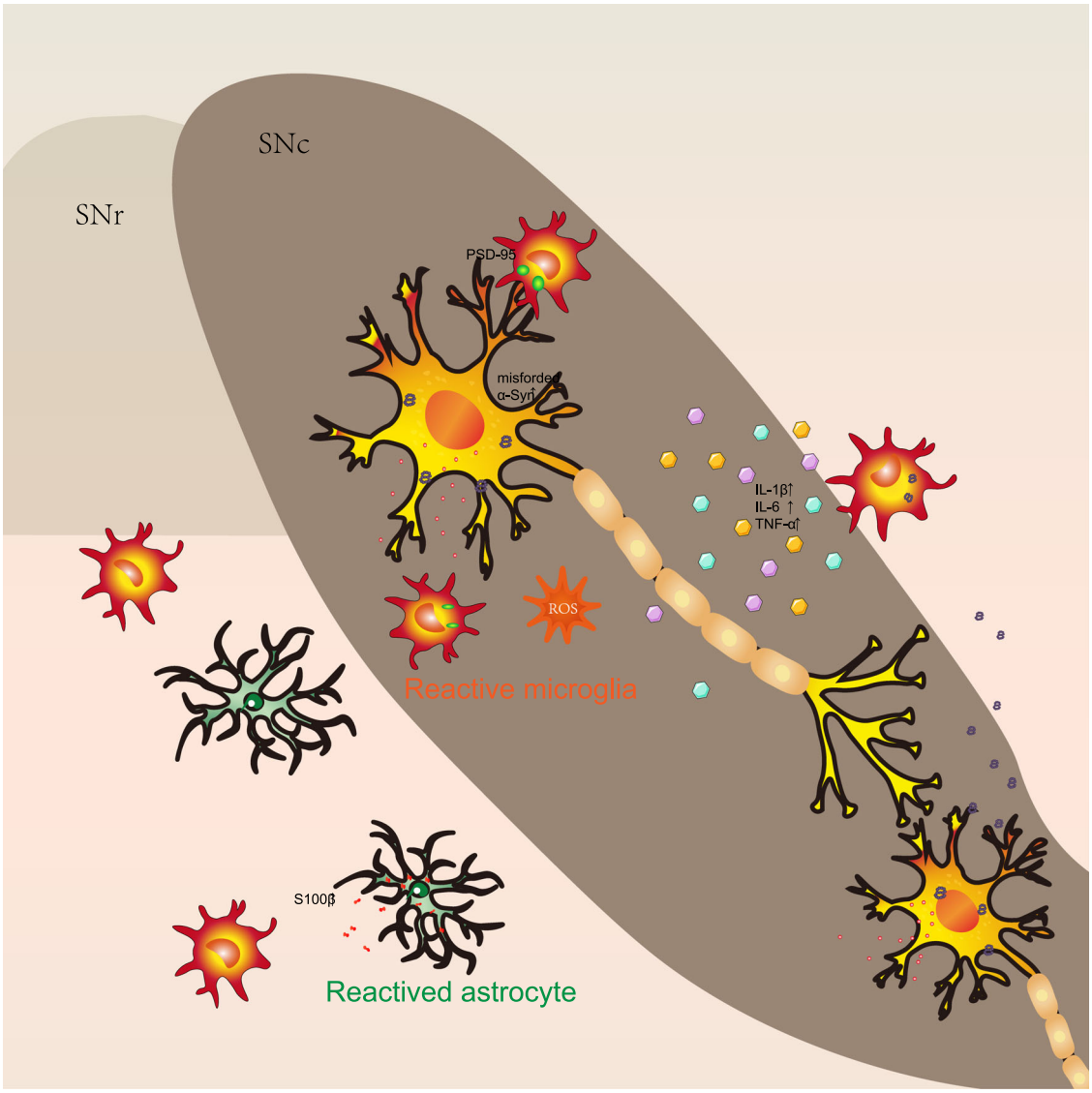

Fig. 8 Schematic diagram of the effect of TBI on neurons and glial cells in the SNc. TBI results in the apoptosis of dopaminergic cells which led to the PD-like behavior in the 6MPI. The accumulation of α-Syn and cytoplasm translocation of TDP43 accounted for the neuronal damage in the SNc post injury. In line with the apoptotic dopaminergic neurons, chronic neuroinflammation was supported by the reactive astrocytes and microgliosis, enhancement of proinflammatory factors, the engulfment of synapsin by reactive microglia in ipsilateral SNc.

neurons over time. It has been reported that the misfolded of α-Syn with neurotoxic activity induce glial activation [49]. Conversely, inflammation would take effect on the biological toxicity of α-Syn, leading to detrimental consequences for neurotoxic processes [50]. Besides, it has been proven that mislocalization of TDP-43 from the nucleus to the cytoplasm is pathological hallmark of various major neurodegenerative diseases [51]. Either insufficient nuclear levels or elevated cytoplasmic levels of TDP43 are directly related to neuronal dysfunction and cytotoxicity [52]. Our study revealed that TDP-43 was translocated into the cytoplasm of TH-positive neurons of chronic TBI, suggesting a causal nexus between mislocalized TDP-43 and the development of PD phenotype. Interestingly, TDP-43 and α-Synuclein were also found to co-localize in the SN of PD patients and dementia with

Lewy bodies (DLB), indicating a potential direct interaction between the two proteins [53, 54]. Our data demonstrate that accelerated loss of dopaminergic neurons and time-dependent behavioral impairment correlates with abnormal protein response to a moderate TBI.

Inflammatory responses are major component of secondary injury post TBI [55]. Inflammatory cells accumulate in the injury region after TBI, which releases a large number of inflammatory factors [56]. TBI also leads to chronic neuroinflammation in the remote brain regions besides the sites of injury [57]. Ilknur Ozen found that mice subjected to TBI had increased microglia activation in the globus pallidus, and neutralization of IL-1β attenuated the microglia activation [58]. Previous studies of animal models showed that inflammation factors, like IL-1β, IL6 and TNF-α were upregulated in SN of patients with PD and neurotoxin-treated animal models of PD [59, 60]. Besides, inhibition of IL-1β has been proven to prevent α-Syn pathology and dopaminergic neurodegeneration in mouse models of PD [61]. Our present study also demonstrated that cortical injury led to the production of proinflammatory cytokines in the SN. Previous report has indicated that a diverse array of cytotoxic factors such as TNF-α, IL-1β and IL-6 contribute to the pathological deposition of TDP-43 through the amplification of a series of cascade reactions [51]. Indeed, dopaminergic neurons seem particularly vulnerable to inflammatory cytokines [62]. Inhibition of soluble TNF signaling with a dominant-negative TNF inhibitor resulted in approximately 50% improvement in dopaminergic neuron survival in several preclinical models of PD [63]. Although we do not how these proinflammatory cytokines form a complex network of inflammatory mediators that propagate an inflammatory response within the damaged tissue, the persistence of inflammation in the ipsilateral SN may contribute to the PD-like behavior dysfunction in middle-aged mice.

Both astrocytes and microglia after TBI may be activated immediately, causing neuroinflammation and brain damage [56]. To delve into the inflammatory reaction, we observed that reactive astrocytes mainly presented in the substantia nigra reticular layer (SNr), as previously reported that GFAP expression was weaker in the overlying SNc [64, 65]. Regional differences in astrocytes may contribute to selective vulnerability in PD. Several postmortem studies found that reduced astrocyte densities may be related to PD and α-Syn-positive inclusions have been identified in astrocytes [66]. Previous research has demonstrated that astrocytes stored and to some extent transfer aggregated α-Syn to neighboring astrocytes, rather than degraded it. The accumulation of α-Syn aggregates in astrocytes disrupts their functions, including glutamate uptake and regulation of the blood-brain barrier [67]. Furthermore, astrocytes primarily transform into A1 neurotoxic astrocytes, which may setup the toxic environment and detrimental to neuronal function [65, 68]. Moreover, inhibiting the microglia-driven differentiation of C3+ neurotoxic astrocytes can prevent dopaminergic neuron loss and mitigate behavioral deficits in preclinical PD mouse models [69]. However, the excessive activation of astrocytes in the SNr is related to glial scar formation, which is thought to inhibit axonal projections of dopaminergic neurons from the SNc to the SNr. Additionally, our data showed that extensive morphological remodeling of astrocytes occurred in the SN during the chronic phase of TBI. Notably, astrocyte axon retraction was observed at 6 months post-injury, suggesting a loss of support for neurons. This finding is consistent with the previous report indicating that TBI causes the formation of complex spatial structures by astrocytes [70].

In recent studies, TBI triggers microglia activation during acute and chronic time points [16, 17, 20]. In vivo imaging has demonstrated that activated microglia are present in the early stage of PD and long-lasting activation and inflammatory responses in the brain are positively correlated with disease progression [71]. The phagocytosis of activated microglia maintains brain homeostasis via the clearance of cellular debris and potential synaptic pruning [72, 73]. However, abnormal α-Syn is known to induce microglial hyperactivation and associated negative effects on synaptic function and mitochondrial homeostasis, which may contribute to the pathogenesis of neurodegenerative diseases [74]. Our findings demonstrated that the M1 subtype of microglia was a chronic and potentially lifelong event in the SN post injury. Transcription factors activated by M1-like microglia trigger upregulation of pro-inflammatory cell surface markers, such as CD16 and CD86 [75]. In addition, this microglia-derived inflammation may prompt astrocytes to adopt neurotoxic functions or to lose their neurotrophic and synaptoptrophic functionality [76]. This pro-inflammatory response could be a significant contributing factor to the initiation of dopaminergic neurodegeneration. In addition to the pro-inflammatory phenotype, the varying phagocytic dynamics of microglia may be associated with the TBI-triggered molecular events on PD-like pathology. A postmortem study of PD patients revealed a disease-specific increase in amoeboid shape of microglia in SN compared to healthy controls indicating their reactive state [77]. Our data showed that similar morphological changes in microglia occurred in the SN during the chronic phase of TBI, characterized by larger cell somas and shorter processes. Numerous evidence reveal that microglia activation contributes to complement-mediated synapse loss in neurodegenerative diseases [78–81]. The upregulation of CD68 in reactive microglia would engulf synapses in the chronic TBI, which was supported by the PSD95-immunoreactive puncta colocalized with microglia in the SNc after 3 months' post-injury. The surviving neurons with significant reduction in dendritic spines and incomplete morphology also indicated the impaired neuronal function [82]. Research involving human brain specimens obtained during autopsy and alongside animal models of PD have revealed that common motor impairments are linked to the reduction in dendrite size, of dendritic spines, and irregular spine structures in the medium spiny neurons of the striatum [83].

Our present study disclosed the progression and pathogenesis of PD-like behavior at different intervals in chronic TBI mice. Nevertheless, there are many constrains should be noted. Age is an essential determinant in the susceptibility to PD. The primary objective of our study was to examine PD-like neurological dysfunction after TBI, which was aggravated in middle-aged mice. Further study should be conducted to explore the consequences of aging post TBI. Furthermore, our data revealed the PD-like behavior and pathology post TBI, the neuroinflammation would play a critical role in the pathogenesis of Parkinson's disease. It is imperative to do some additional research to explore the pertinent molecular mechanism.

CONCLUSION

The present data described the progressive PD-like behaviors and pathology that occur post TBI. The deleterious effects on dopaminergic neurons were associated with the buildup of misfolded protein, heightened neuroinflammation and increased microglial phagocytosis. The current study offers valuable insights into the potential mechanism that contributes to the increased risk of PD post TBI.

DATA AVAILABILITY

Correspondence and requests for materials should be addressed to SG, GL, RZ and YT.

REFERENCES

1. Sun CP, Zhou JJ, Yu ZL, Huo XK, Zhang J, Morisseau C, et al. Kurarinone alleviated Parkinson's disease via stabilization of epoxyeicosatrienoic acids in animal model. Proc Natl Acad Sci USA. 2022;119:e2118818119.
2. Prunell G, Olivera-Bravo S. A focus on astrocyte contribution to Parkinson's disease etiology. Biomolecules. 2022;12:1745.

3. Maas AIR, Menon DK, Manley GT, Abrams M, Akerlund C, Andelic N, et al. Traumatic brain injury: progress and challenges in prevention, clinical care, and research. Lancet Neurol. 2022;21:1004–60.
4. Delic V, Beck KD, Pang KCH, Citron BA. Biological links between traumatic brain injury and Parkinson's disease. Acta Neuropathol Commun. 2020;8:45.
5. Crane PK, Gibbons LE, Dams-O'Connor K, Trittschuh E, Leverenz JB, Keene CD, et al. Association of traumatic brain injury with late-life neurodegenerative conditions and neuropathologic findings. JAMA Neurol. 2016;73:1062–9.
6. Acosta G, Race N, Herr S, Fernandez J, Tang J, Rogers E, et al. Acrolein-mediated alpha-synuclein pathology involvement in the early post-injury pathogenesis of mild blast-induced Parkinsonian neurodegeneration. Mol Cell Neurosci. 2019;98:140–54.
7. Gardner RC, Byers AL, Barnes DE, Li Y, Boscardin J, Yaffe K. Mild TBI and risk of Parkinson disease: a chronic effects of neurotrauma consortium study. Neurology. 2018;90:e1771–e79.
8. Jafari S, Etminan M, Aminzadeh F, Samii A. Head injury and risk of Parkinson disease: a systematic review and meta-analysis. Mov Disord. 2013;28:1222–9.
9. Gardner RC, Burke JF, Nettiksimmons J, Goldman S, Tanner CM, Yaffe K. Traumatic brain injury in later life increases risk for Parkinson disease. Ann Neurol. 2015;77:987–95.
10. Morissette MP, Prior HJ, Tate RB, Wade J, Leiter JRS. Associations between concussion and risk of diagnosis of psychological and neurological disorders: a retrospective population-based cohort study. Fam Med Community Health. 2020;8:e000390.
11. Tan L, Ge H, Tang J, Fu C, Duanmu W, Chen Y, et al. Amantadine preserves dopamine level and attenuates depression-like behavior induced by traumatic brain injury in rats. Behav Brain Res. 2015;279:274–82.
12. Ascherio A, Schwarzschild MA. The epidemiology of Parkinson's disease: risk factors and prevention. Lancet Neurol. 2016;15:1257–72.
13. Taylor KM, Saint-Hilaire MH, Sudarsky L, Simon DK, Hersh B, Sparrow D, et al. Head injury at early ages is associated with risk of Parkinson's disease. Parkinsonism Relat Disord. 2016;23:57–61.
14. Dickson DW, Braak H, Duda JE, Duyckaerts C, Gasser T, Halliday GM, et al. Neuropathological assessment of Parkinson's disease: refining the diagnostic criteria. Lancet Neurol. 2009;8:1150–7.
15. Sonustun B, Altay MF, Strand C, Ebanks K, Hondhamuni G, Warner TT, et al. Pathological relevance of post-translationally modified alpha-synuclein (pSer87, pSer129, nTyr39) in Idiopathic Parkinson's disease and multiple system atrophy. Cells. 2022;11:906.
16. Liu M, Bachstetter AD, Cass WA, Lifshitz J, Bing G. Pioglitazone attenuates neuroinflammation and promotes dopaminergic neuronal survival in the nigrostriatal system of rats after diffuse brain injury. J Neurotrauma. 2017;34:414–22.
17. Impellizzeri D, Campolo M, Bruschetta G, Crupi R, Cordaro M, Paterniti I, et al. Traumatic brain injury leads to development of Parkinson's disease related pathology in mice. Front Neurosci. 2016;10:458.
18. Corps KN, Roth TL, McGavern DB. Inflammation and neuroprotection in traumatic brain injury. JAMA Neurol. 2015;72:355–62.
19. van Bregt DR, Thomas TC, Hinzman JM, Cao T, Liu M, Bing G, et al. Substantia nigra vulnerability after a single moderate diffuse brain injury in the rat. Exp Neurol. 2012;234:8–19.
20. Hutson CB, Lazo CR, Mortazavi F, Giza CC, Hovda D, Chesselet MF. Traumatic brain injury in adult rats causes progressive nigrostriatal dopaminergic cell loss and enhanced vulnerability to the pesticide paraquat. J Neurotrauma. 2011;28:1783–801.
21. San Luciano M, Tanner CM, Meng C, Marras C, Goldman SM, Lang AE, et al. Nonsteroidal anti-inflammatory use and LRRK2 Parkinson's disease penetrance. Mov Disord. 2020;35:1755–64.
22. Karve IP, Taylor JM, Crack PJ. The contribution of astrocytes and microglia to traumatic brain injury. Br J Pharmacol. 2016;173:692–702.
23. Kiyota T, Machhi J, Lu Y, Dyavarshetty B, Nemati M, Zhang G, et al. URMC-099 facilitates amyloid-β clearance in a murine model of Alzheimer's disease. J Neuroinflammation. 2018;15:137.
24. Ham HJ, Han SB, Yun J, Yeo IJ, Ham YW, Kim SH, et al. Bee venom phospholipase A2 ameliorates amyloidogenesis and neuroinflammation through inhibition of signal transducer and activator of transcription-3 pathway in Tg2576 mice. Transl Neurodegener. 2019;8:26.
25. Cheng H, Wang N, Ma X, Wang P, Dong W, Chen Z, et al. Spatial-temporal changes of iron deposition and iron metabolism after traumatic brain injury in mice. Front Mol Neurosci. 2022;15:949573.
26. Kaur A, Jaiswal G, Brar J, Kumar P. Neuroprotective effect of nerolidol in traumatic brain injury associated behavioural comorbidities in rats. Toxicol Res. 2021;10:40–50.
27. Yu H, Liu X, Chen B, Vickstrom CR, Friedman V, Kelly TJ, et al. The neuroprotective effects of the CB2 agonist GW842166x in the 6-OHDA mouse model of Parkinson's disease. Cells. 2021;10:3548.
28. Castro B, Kuang S. Evaluation of muscle performance in mice by treadmill exhaustion test and whole-limb grip strength assay. Bio Protoc. 2017;7:e2237.
29. Sakhaee E, Ostadhadi S, Khan MI, Yousefi F, Norouzi-Javidan A, Akbarian R, et al. The role of NMDA receptor and nitric oxide/cyclic guanosine monophosphate pathway in the antidepressant-like effect of dextromethorphan in mice forced swimming test and tail suspension test. Biomed Pharmacother. 2017;85:627–34.
30. Chuang CS, Su HL, Cheng FC, Hsu SH, Chuang CF, Liu CS. Quantitative evaluation of motor function before and after engraftment of dopaminergic neurons in a rat model of Parkinson's disease. J Biomed Sci. 2010;17:9.
31. Ritzel RM, Li Y, Lei Z, Carter J, He J, Choi HMC, et al. Functional and transcriptional profiling of microglial activation during the chronic phase of TBI identifies an age-related driver of poor outcome in old mice. GeroScience. 2022;44:1407–40.
32. Bisht R, Kaur B, Gupta H, Prakash A. Ceftriaxone mediated rescue of nigral oxidative damage and motor deficits in MPTP model of Parkinson's disease in rats. Neurotoxicology. 2014;44:71–9.
33. Bondi H, Bortolotto V, Canonico PL, Grilli M. Complex and regional-specific changes in the morphological complexity of GFAP(+) astrocytes in middle-aged mice. Neurobiol Aging. 2021;100:59–71.
34. Goedert M. Neurodegeneration. Alzheimer's and Parkinson's diseases: the prion concept in relation to assembled abeta, tau, and alpha-synuclein. Science. 2015;349:1255555.
35. Dionisio PA, Amaral JD, Rodrigues CMP. Oxidative stress and regulated cell death in Parkinson's disease. Ageing Res Rev. 2021;67:101263.
36. Walker AK, Spiller KJ, Ge G, Zheng A, Xu Y, Zhou M, et al. Functional recovery in new mouse models of ALS/FTLD after clearance of pathological cytoplasmic TDP-43. Acta Neuropathol. 2015;130:643–60.
37. Gasset-Rosa F, Lu S, Yu H, Chen C, Melamed Z, Guo L, et al. Cytoplasmic TDP-43 de-mixing independent of stress granules drives inhibition of nuclear import, loss of nuclear TDP-43, and cell death. Neuron. 2019;102:339–57.
38. Mercurio D, Fumagalli S, Schafer MK, Pedragosa J, Ngassam LDC, Wilhelmi V, et al. Protein expression of the microglial marker Tmem119 decreases in association with morphological changes and location in a mouse model of traumatic brain injury. Front Cell Neurosci. 2022;16:820127.
39. Kesavan C, Bajwa NM, Watt H, Mohan S. Experimental repetitive mild traumatic brain injury induces deficits in trabecular bone microarchitecture and strength in mice. Bone Res. 2017;5:17042.
40. Samii A, Nutt JG, Ransom BR. Parkinson's disease. Lancet. 2004;363:1783–93.
41. Mao X, Terpolilli NA, Wehn A, Cheng S, Hellal F, Liu B, et al. Progressive histopathological damage occurring up to one year after experimental traumatic brain injury is associated with cognitive decline and depression-like behavior. J Neurotrauma. 2020;37:1331–41.
42. Winogrodzka A, Wagenaar RC, Booij J, Wolters EC. Rigidity and bradykinesia reduce interlimb coordination in Parkinsonian gait. Arch Phys Med Rehabil. 2005;86:183–9.
43. Koch JC, Bitow F, Haack J, d'Hedouville Z, Zhang JN, Tonges L, et al. Alpha-synuclein affects neurite morphology, autophagy, vesicle transport and axonal degeneration in CNS neurons. Cell Death Dis. 2015;6:e1811.
44. Cronin-Furman EN, Barber-Singh J, Bergquist KE, Yagi T, Trimmer PA. Differential effects of yeast NADH dehydrogenase (Ndi1) expression on mitochondrial function and inclusion formation in a cell culture model of sporadic Parkinson's disease. Biomolecules. 2019;9:119.
45. Pinto M, Nissanka N, Peralta S, Brambilla R, Diaz F, Moraes CT. Pioglitazone ameliorates the phenotype of a novel Parkinson's disease mouse model by reducing neuroinflammation. Mol Neurodegener. 2016;11:25.
46. Acosta SA, Tajiri N, de la Pena I, Bastawrous M, Sanberg PR, Kaneko Y, et al. Alpha-synuclein as a pathological link between chronic traumatic brain injury and Parkinson's disease. J Cell Physiol. 2015;230:1024–32.
47. Kokiko-Cochran O, Ransohoff L, Veenstra M, Lee S, Saber M, Sikora M, et al. Altered neuroinflammation and behavior after traumatic brain injury in a mouse model of Alzheimer's disease. J Neurotrauma. 2016;33:625–40.
48. Ferrer-Lorente R, Lozano-Cruz T, Fernández-Carasa I, Miłowska K, de la Mata FJ, Bryszewska M, et al. Cationic carbosilane dendrimers prevent abnormal α-synuclein accumulation in Parkinson's disease patient-specific dopamine neurons. Biomacromolecules. 2021;22:4582–91.
49. La Vitola P, Balducci C, Cerovic M, Santamaria G, Brandi E, Grandi F, et al. Alpha-synuclein oligomers impair memory through glial cell activation and via toll-like receptor 2. Brain Behav Immun. 2018;69:591–602.
50. Choi I, Zhang Y, Seegobin SP, Pruvost M, Wang Q, Purtell K, et al. Microglia clear neuron-released α-synuclein via selective autophagy and prevent neurodegeneration. Nat Commun. 2020;11:1386.
51. Liao YZ, Ma J, Dou JZ. The role of TDP-43 in neurodegenerative disease. Mol Neurobiol. 2022;59:4223–41.
52. Tziortzouda P, Van Den Bosch L, Hirth F. Triad of TDP43 control in neurodegeneration: autoregulation, localization and aggregation. Nat Rev Neurosci. 2021;22:197–208.
53. Kokoulina P, Rohn TT. Caspase-cleaved transactivation response DNA-binding protein 43 in Parkinson's disease and dementia with lewy bodies. Neurodegener Dis. 2010;7:243–50.
54. Chhangani D, Martin-Pena A, Rincon-Limas DE. Molecular, functional, and pathological aspects of TDP-43 fragmentation. iScience. 2021;24:102459.

55. Chen J, Wang X, Hu J, Du J, Dordoe C, Zhou Q, et al. FGF20 protected against BBB disruption after traumatic brain injury by upregulating junction protein expression and inhibiting the inflammatory response. Front Pharmacol. 2020;11:590669.
56. Saeed K, Jo MH, Park JS, Alam SI, Khan I, Ahmad R, et al. 17β-estradiol abrogates oxidative stress and neuroinflammation after cortical stab wound injury. Antioxidants. 2021;10:1682.
57. Erturk A, Mentz S, Stout EE, Hedehus M, Dominguez SL, Neumaier L, et al. Interfering with the chronic immune response rescues chronic degeneration after traumatic brain injury. J Neurosci. 2016;36:9962–75.
58. Ozen I, Ruscher K, Nilsson R, Flygt J, Clausen F, Marklund N. Interleukin-1 beta neutralization attenuates traumatic brain injury-induced microglia activation and neuronal changes in the globus pallidus. Int J Mol Sci. 2020;21:387.
59. Zhao Z, Ning J, Bao XQ, Shang M, Ma J, Li G, et al. Fecal microbiota transplantation protects rotenone-induced Parkinson's disease mice via suppressing inflammation mediated by the lipopolysaccharide-TLR4 signaling pathway through the microbiota-gut-brain axis. Microbiome. 2021;9:226.
60. Mogi M, Harada M, Riederer P, Narabayashi H, Fujita K, Nagatsu T. Tumor necrosis factor-alpha (TNF-alpha) increases both in the brain and in the cerebrospinal fluid from parkinsonian patients. Neurosci Lett. 1994;165:208–10.
61. Gordon R, Albornoz EA, Christie DC, Langley MR, Kumar V, Mantovani S, et al. Inflammasome inhibition prevents α-synuclein pathology and dopaminergic neurodegeneration in mice. Sci Transl Med. 2018;10:eaah4066.
62. Levesque S, Wilson B, Gregoria V, Thorpe LB, Dallas S, Polikov VS, et al. Reactive microgliosis: extracellular micro-calpain and microglia-mediated dopaminergic neurotoxicity. Brain. 2010;133:808–21.
63. Marogianni C, Sokratous M, Dardiotis E, Hadjigeorgiou GM, Bogdanos D, Xiromerisiou G. Neurodegeneration and inflammation-an interesting interplay in Parkinson's disease. Int J Mol Sci. 2020;21:8421.
64. Crittenden JR, Tillberg PW, Riad MH, Shima Y, Gerfen CR, Curry J, et al. Striosome-dendron bouquets highlight a unique striatonigral circuit targeting dopamine-containing neurons. Proc Natl Acad Sci USA. 2016;113:11318–23.
65. Basurco L, Abellanas MA, Ayerra L, Conde E, Vinueza-Gavilanes R, Luquin E, et al. Microglia and astrocyte activation is region-dependent in the alpha-synuclein mouse model of Parkinson's disease. Glia. 2023;71:571–87.
66. Braak H, Sastre M, Del Tredici K. Development of alpha-synuclein immunoreactive astrocytes in the forebrain parallels stages of intraneuronal pathology in sporadic Parkinson's disease. Acta Neuropathol. 2007;114:231–41.
67. Wang C, Yang T, Liang M, Xie J, Song N. Astrocyte dysfunction in Parkinson's disease: from the perspectives of transmitted alpha-synuclein and genetic modulation. Transl Neurodegener. 2021;10:39.
68. Brandebura AN, Paumier A, Onur TS, Allen NJ. Astrocyte contribution to dysfunction, risk and progression in neurodegenerative disorders. Nat Rev Neurosci. 2023;24:23–39.
69. Yun SP, Kam TI, Panicker N, Kim S, Oh Y, Park JS, et al. Block of A1 astrocyte conversion by microglia is neuroprotective in models of Parkinson's disease. Nat Med. 2018;24:931–38.
70. Chen Z, Wang P, Cheng H, Wang N, Wu M, Wang Z, et al. Adolescent traumatic brain injury leads to incremental neural impairment in middle-aged mice: role of persistent oxidative stress and neuroinflammation. Front Neurosci. 2023;17:1292014.
71. Wendimu MY, Hooks SB. Microglia phenotypes in aging and neurodegenerative diseases. Cells. 2022;11:2091.
72. Delage C, Taib T, Mamma C, Lerouet D, Besson VC. Traumatic brain injury: an age-dependent view of post-traumatic neuroinflammation and its treatment. Pharmaceutics. 2021;13:1624.
73. Luo R, Su LY, Li G, Yang J, Liu Q, Yang LX, et al. Activation of PPARA-mediated autophagy reduces Alzheimer disease-like pathology and cognitive decline in a murine model. Autophagy. 2020;16:52–69.
74. Scheiblich H, Bousset L, Schwartz S, Griep A, Latz E, Melki R, et al. Microglial NLRP3 Inflammasome activation upon TLR2 and TLR5 ligation by distinct alpha-synuclein assemblies. J Immunol. 2021;207:2143–54.
75. Feng S, Wu C, Zou P, Deng Q, Chen Z, Li M, et al. High-intensity interval training ameliorates Alzheimer's disease-like pathology by regulating astrocyte phenotype-associated AQP4 polarization. Theranostics. 2023;13:3434–50.
76. Kam TI, Hinkle JT, Dawson TM, Dawson VL. Microglia and astrocyte dysfunction in parkinson's disease. Neurobiol Dis. 2020;144:105028.
77. Smajić S, Prada-Medina CA, Landoulsi Z, Ghelfi J, Delcambre S, Dietrich C, et al. Single-cell sequencing of human midbrain reveals glial activation and a Parkinson-specific neuronal state. Brain. 2022;145:964–78.
78. Laurent C, Dorothée G, Hunot S, Martin E, Monnet Y, Duchamp M, et al. Hippocampal T cell infiltration promotes neuroinflammation and cognitive decline in a mouse model of tauopathy. Brain. 2017;140:184–200.
79. Liu YU, Ying Y, Li Y, Eyo UB, Chen T, Zheng J, et al. Neuronal network activity controls microglial process surveillance in awake mice via norepinephrine signaling. Nat Neurosci. 2019;22:1771–81.
80. Xu Y, Jiang C, Wu J, Liu P, Deng X, Zhang Y, et al. Ketogenic diet ameliorates cognitive impairment and neuroinflammation in a mouse model of Alzheimer's disease. CNS Neurosci Ther. 2022;28:580–92.
81. Hammond JW, Bellizzi MJ, Ware C, Qiu WQ, Saminathan P, Li H, et al. Complement-dependent synapse loss and microgliosis in a mouse model of multiple sclerosis. Brain Behav Immun. 2020;87:739–50.
82. Dell'Orco JM, Wasserman AH, Chopra R, Ingram MA, Hu YS, Singh V, et al. Neuronal atrophy early in degenerative ataxia is a compensatory mechanism to regulate membrane excitability. J Neurosci. 2015;35:11292–307.
83. Herms J, Dorostkar MM. Dendritic spine pathology in neurodegenerative diseases. Annu Rev Pathol. 2016;11:221–50.

AUTHOR CONTRIBUTIONS

RS and MW performed the research, analyzed the data, and wrote the manuscript; PW and SG contributed to data interpretation and provided valuable input in the preparation of the manuscript. GL, ZC, WL and SW performed the experiments and collected the data; SG, GL, RZ and YT designed the study and edited the manuscript. All authors reviewed, contributed and approved the final manuscript.

FUNDING

This work was supported by grant from the Liaoning Province Applied Basic Research Program (2022JH2/101300055 to YQT, 2023JH2/101700104 to SG), National Natural Science Foundation of China (81971793, 82371894 to RZ), and Liaoning Natural Science Foundation (2022-YGJC-74 to RZ).

COMPETING INTERESTS

The authors declare no competing interests.

ETHICS APPROVAL AND CONSENT TO PARTICIPATE

This study was approved by the Ethics Committee of China Medical University (Approval No. CMU2020315) and performed in accordance with the National Institutes of Health Laboratory Animal Care and Use Guidelines (NIH Publication No. 80-23). The manuscript was written in accordance with the Animal Research: Reporting In vivo Experiments (ARRIVE) guidelines.

ADDITIONAL INFORMATION

Supplementary information The online version contains supplementary material available at https://doi.org/10.1038/s41398-025-03232-7.

Correspondence and requests for materials should be addressed to Shun Gong, Guobiao Liang, Rui Zhao or Yingqun Tao.